Reconstruction and Motion Estimation from Apparent Contours under Circular Motion

K-Y. K. Wong, P. R. S. Mendonça and R. Cipolla
Department of Engineering
University of Cambridge
Cambridge, UK, CB2 1PZ
[kykw2|prdsm2|cipolla]@eng.cam.ac.uk

Abstract

In this paper we address the problem of recovering structure and motion from the contours of a smooth-curved surface. A novel and simpler technique for computing the structure of an object from its profiles is introduced. Experiments with real data show encouraging results, which are comparable to those obtained from much more sophisticated techniques. Furthermore, a new method for motion estimation from sequences of profiles is proposed. Preliminary results demonstrate the feasibility of the algorithm.

1 Introduction

The recovering of structure and motion from sequences of images is a central problem in computer vision, and its solution has generated a rich pool of algorithms [8, 1]. Most of these algorithms rely on correspondences of points or lines between images, and work well when the scene being viewed is composed of polyhedral parts. However, for smooth surfaces without noticeable texture, point and line correspondences may not be easily established. In this case the profile of the surface is, very often, the only feature available. This calls for the development of a completely different set of techniques, as the ones found in [17, 16, 19, 5, 2, 18].

In this paper we address the problem of structure and motion recovery from the profiles of smooth surfaces. In section 2, the differential geometry of surface will first be briefly reviewed. This forms the theoretical framework for various techniques developed for the reconstruction of surfaces from profiles. Existing methods for reconstruction from discrete viewpoints are then described and compared. A simple and basic method for reconstruction is proposed and experimental results are presented, showing that the model recovered by this simple method is comparable to the others. The problem of motion estimation is tackled in section 3, where a novel technique, based on properties of the affine epipolar geometry under circular motion, is introduced. Experiments with synthetic data demonstrating the feasibility of the method have been carried out, and preliminary results are presented.

2 Reconstruction from Apparent Contours

2.1 Surface Geometry

Consider a point P on a smooth-curved surface S. Under perspective projection the vector position $\mathbf{r}$ of P is given by $\mathbf{r} = \mathbf{c} + \lambda\mathbf{p}$, where $\mathbf{c}$ is the camera centre position, $\mathbf{p}$ is the unit viewing direction and λ is the depth of the point P along the viewing direction $\mathbf{p}$. For a given camera centre position $\mathbf{c}$, the set of points $\mathbf{r}$ on the surface for which the visual ray is tangent to S is called the contour generator and must satisfy $\mathbf{p} \cdot \mathbf{n} = 0$, where $\mathbf{n}$ is the unit normal to the surface S at $\mathbf{r}$. The contour generator depends on both local surface geometry and camera position, and its projection onto the image plane is called the apparent contour, which forms the profile of the surface in the image.

As the camera moves, the contour generator sweeps over the visible surface. Thus the surface S can be parameterised by this spatio-temporal surface swept out by the contour generators as a result of the camera motion

$$\mathbf{r}(s,t) = \mathbf{c}(t) + \lambda(s,t)\mathbf{p}(s,t), \quad (1)$$

$$\mathbf{p}(s,t) \cdot \mathbf{n}(s,t) = 0, \quad (2)$$

where the parameter s describes the position along the contour generator while the parameter t corresponds to time. Such a parameterisation is however under-constrained: curves of constant t are the contour generators with camera centre positions $\mathbf{c}(t)$, while curves of constant s have no physical interpretation. The most widely used parameterisation is the epipolar parameterisation [4] (see fig. 1) which is derived from the epipolar geometry in stereo vision: two points on two successive contour generators are correspondent if they both lie in the epipolar plane defined by the two camera centre positions and one of the points. Below the subscripts s and t represents the spatial and temporal derivatives

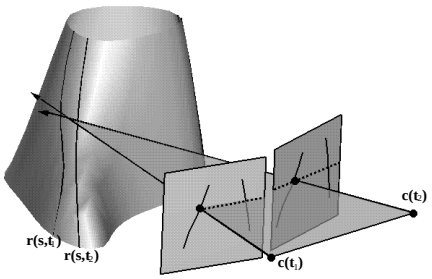

Figure 1: Epipolar parameterisation for the spatial-temporal surface swept by the contour generators.

respectively. By differentiating (1) with respect to s and taking the scalar product with the normal $\mathbf{n}(s,t)$, and combining with (2) and $\mathbf{r}_s \cdot \mathbf{n}(s,t) = 0$, we have $\mathbf{p}_s \cdot \mathbf{n}(s,t) = 0$. Thus the surface normal can be recovered from the apparent contour up to a sign by

$$\mathbf{n}(s,t) = \frac{\mathbf{p}(s,t) \wedge \mathbf{p}_s}{|\mathbf{p}(s,t) \wedge \mathbf{p}_s|}. \quad (3)$$

Finally, by differentiating (1) with respect to t and taking the scalar product with the normal $\mathbf{n}(s,t)$, and combining with (2) and $\mathbf{r}_t \cdot \mathbf{n}(s,t) = 0$, depth $\lambda(s,t)$, and thus the

3D structure $\mathbf{r}(s,t)$, can be recovered by [4]

$$\lambda(s,t) \quad = \quad -\frac{\mathbf{c}_t \cdot \mathbf{n}(s,t)}{\mathbf{p}_t \cdot \mathbf{n}(s,t)}. \tag{4}$$

2.2 Discrete Viewpoints

The depth formula (4) requires a dense continuous image sequence for approximating the spatial and temporal derivatives, and is sensitive to edge localisation. However, in practice only images at discrete viewpoints will be available and thus (4) cannot be used directly.

Cipolla and Blake [5] developed a simple numerical method for estimating depth from a minimum of three discrete views by determining the osculating circle in each epipolar plane. Given three correspondences in three consecutive apparent contours, the viewing lines defined by them are projected onto the epipolar plane defined by the first two. By assuming that the curvature of the epipolar curve $\mathbf{r}(s_0,t)$ is locally constant, it can be approximated as part of a circle tangent to these viewing lines. Vaillant and Faugeras [19] developed a similar algorithm which uses the radial plane instead of the epipolar plane. The osculating circle methods require the camera motion to be close to linear and the surface remains on the same side of the tangents in the projection plane.

Boyer and Berger [2] derived a depth formulation from a local approximation of the surface up to order two. Given two corresponding points P_1 and P_2 on two successive contour generators with vector positions $\mathbf{r}_1 = \mathbf{c}_1 + \lambda_1 \mathbf{p}_1$ and $\mathbf{r}_2 = \mathbf{c}_2 + \lambda_2 \mathbf{p}_2$, by taking the scalar product of the difference with the normal $\mathbf{n}_2$ to the surface at P_2, we have

$$\lambda_1 \quad = \quad -\frac{\Delta\mathbf{c} \cdot \mathbf{n}_2}{\Delta\mathbf{p} \cdot \mathbf{n}_2} + \frac{\Delta\mathbf{r} \cdot \mathbf{n}_2}{\Delta\mathbf{p} \cdot \mathbf{n}_2}, \tag{5}$$

where $\Delta\mathbf{c} = \mathbf{c}_1 - \mathbf{c}_2$ and likewise for $\Delta\mathbf{r}$ and $\Delta\mathbf{p}$. The second term in (5) involves $\Delta\mathbf{r}$ which is the distance between P_1 and P_2 and cannot be computed, a priori, from measurements in two images. Based on a local surface model with a second order approximation, $\Delta\mathbf{r} \cdot \mathbf{n}_2$ can be expressed in terms of the normal curvature along the viewing direction. This allows the local shape to be estimated from three consecutive contours by solving a pair of simultaneous equations of the form (5). It only requires that the surfaces are at least C^2 and are not locally planar.

In this paper, we propose to use simple triangulation techniques for reconstruction of the curved surface. The epipolar parameterisation of the spatial-temporal surface is adopted and points on consecutive apparent contours are matched according to the epipolar correspondence. The space point can then be obtained by a least square solution to the triangulation problem. This method is indeed a finite-difference (discrete) approximation to (4). Let λ_1 and λ_2 be the distances between the intersection point $\mathbf{q}$ and the two camera centre positions $\mathbf{c}_1$ and $\mathbf{c}_2$ along the viewing directions $\mathbf{p}_1$ and $\mathbf{p}_2$ respectively, we have $\mathbf{q} = \mathbf{c}_1 + \lambda_1 \mathbf{p}_1$ and $\mathbf{q} = \mathbf{c}_2 + \lambda_2 \mathbf{p}_2$. By taking the scalar product of the difference with the normal $\mathbf{n}_2$ to the surface at P_2, we have

$$\lambda_1 \quad = \quad -\frac{\Delta\mathbf{c} \cdot \mathbf{n}_2}{\Delta\mathbf{p} \cdot \mathbf{n}_2}. \tag{6}$$

This equation for λ is essentially the first term in (5). In [2], Boyer and Berger criticised that, by omitting the second term involving $\Delta\mathbf{r} \cdot \mathbf{n}_2$ in (5), it is assumed that the contour

generators are not view dependent, which is false, and thus leads to error in depth estimation. In spite of that, if both the local radius of curvature of the surface and the motion of the camera are small, such errors will be negligible and would not affect the general shape recovered (see sec. 2.3). This method is, of course, computationally simpler. Unlike other methods, no decomposition of the 3x4 projection matrix is needed to obtain the calibration matrix for converting image coordinates to the unit viewing vector $\mathbf{p}(s,t)$, making it numerically more stable. Finally, this method can be used with affine cameras which do not have the concept of camera centre position.

2.3 Implementation and Experimental Results

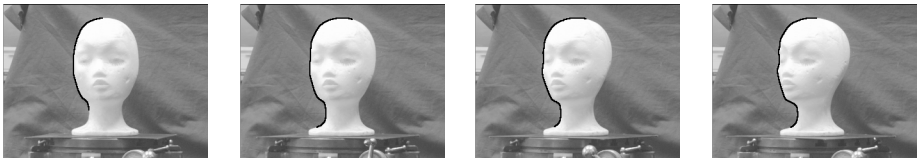

Figure 2: Four consecutive images in the sequence are shown with apparent contours being tracked by cubic B-Spline snakes.

A head model has been reconstructed from the same image sequence using Boyer and Berger's method, finite-difference approximation and simple triangulation respectively. The image sequence was acquired by rotating the head model on a turntable with a fixed camera. The rotation angle between two successive images is of 10° and the whole sequence consists of 36 images. The cameras were calibrated by taking 5 images of a calibration grid performing the same motion on the turntable. Corner features were tracked through the 5 images of the calibration grid and the axis of rotation was estimated by fitting circles to the trajectories of the corner features in space. The projection matrices for the cameras were then generated analytically from the first camera matrix and the axis of rotation. The apparent contours were tracked by using cubic B-spline snakes[4] (see fig. 2). Fundamental matrices [13, 20] between two successive images were formed from the corresponding projection matrices and correspondences were then found by solving for the intersections between epipolar lines and the cubic B-splines analytically and by using ordering and disparity gradient constraints to resolve for any matching ambiguity. The results of the reconstructions are shown in fig. 3.

It can be seen that the contour generators recovered by Boyer and Beger's method are a bit smoother and less noisy. Nonetheless, the models from finite difference approximation and simple triangulation are still comparable to that from Boyer and Berger's method, and the difference is hardly observable after shading. By assuming the radius of curvature d along the epipolar curve be locally constant, the error ξ, which is the distance between the reconstructed point and the surface, is given by

$$\xi = (\sec(\varphi/2) - 1)\, d \approx d\varphi^2/8, \tag{7}$$

where φ is the angle between the viewing directions (see fig. 4). If the camera is far from the rotating object, φ can be approximated by the angle of rotation ω. For ω equals 10°, the error will be 0.38% of the radius d, which will be negligible for small values of d.

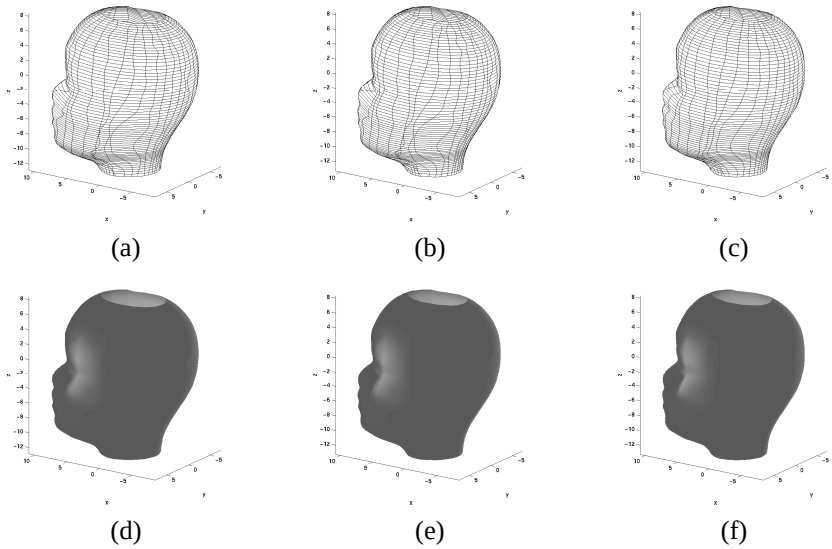

Figure 3: Results of reconstructions. Top row shows the wireframe models and the bottom row shows the models after shading: (a,d) Model built from simple triangulation. (b,e) Model built from finite difference approximation. (c,f) Model built from Boyer and Berger's method.

3 Motion Estimation from Apparent Contours

The fundamental difficulty in estimating the motion of a smooth surface from the sequence of images of its contour generators is that, unlike point or line features [20], the contours do not readily provide image correspondences that allow for the computation of the epipolar geometry, summarised by the fundamental matrix. This characteristic makes the motion estimation difficult even for humans, under certain circumstances [15]. A possible solution to this problem is the use of *epipolar tangencies* [16, 3], as shown in fig. 5. An epipolar tangency is the projection of the *frontier points* [3] (referred to as *fixed points* in [17]), which is the intersection of two consecutive contour generators. If enough epipolar tangencies are present, the epipolar geometry can be estimated, and the motion is determined up to a projective transformation. The intrinsic parameters of the cameras can then be used to fix the motion of the surface [11]. The main problem of this approach is that a minimum of 7 epipolar tangencies are required, a number which is seldom ob-

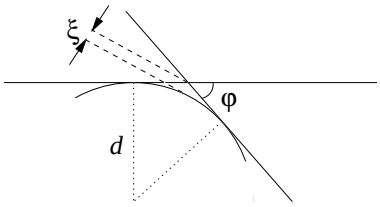

Figure 4: The error ξ between the reconstructed point and the surface is related to the radius of curvature d and the angle φ between the viewing directions.

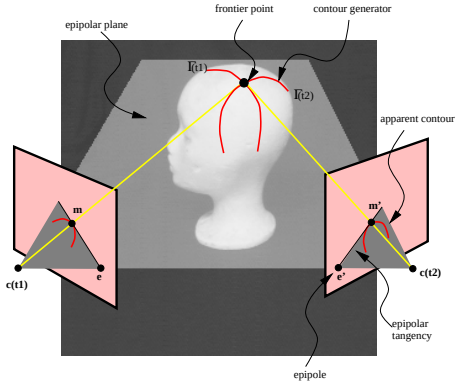

Figure 5: A frontier point is the intersection of two consecutive contour generators and is visible in both views. The frontier point projects to a point on the apparent contour which is an epipolar tangency.

tained in practical circumstances. If the motion and the intrinsic parameters are known to be constant, the epipolar geometry between successive images will also be constant, and epipolar tangencies for successive pairs of images can be used altogether in the estimation of the fundamental matrix. Another possibility is the use of an *affine camera model*, which, as shown in [14], allows for a simpler and more robust estimation of the epipolar geometry from only 4 epipolar tangencies.

The method presented here for motion estimation from apparent contours is a fusion of the techniques introduced in [14]. In these works the main image features of the circular motion, namely the image of the rotation axis and the horizon line [10, 9], are used to derive a parameterisation of the fundamental matrix with only 6 degrees of freedom (d.o.f.), while the affine approximation is used to reduce the space of search of the parameters of the fundamental matrix. The drawback of the first method is that 6 epipolar tangencies are still needed, or 4 images with two epipolar tangencies each if the angle of rotation of the circular motion is fixed. In the affine case, 4 epipolar tangencies are still needed, and, again the use of successive pairs of images is possible only if the motion is constant.

3.1 Theoretical Background

Consider two affine cameras. The orientation of the epipolar lines on each image will depend only on the relative orientation of the normals to the image planes and the *cyclotorsion*, which is the rotation of the cameras around their optical axis. Fig. 6(a) shows a camera rotating an angle ω around an arbitrary (but fixed) axis. The angle between the image of the axis of rotation and the vertical axis in the image plane (in image coordinates) is denoted by θ, as shown in fig. 6(b). The angle between the image plane and the rotation axis is represented in Fig. 6(c) by ψ. It is important to notice that the angles θ and ψ are preserved by the rotation around the fixed axis. Let $\mathbf{k}_1$ and $\mathbf{k}_2$ be the unit vectors corresponding to the directions of the optical axis of the reference camera and the camera rotated by ω, respectively, according to fig. 7(a). It is easy to see that the effect of θ on the orientation α of the epipolar lines is simply to rotate them by θ. Without loss of generality, let θ be equal to zero. To compute α it is necessary to project $\mathbf{k}_2$ back to the reference

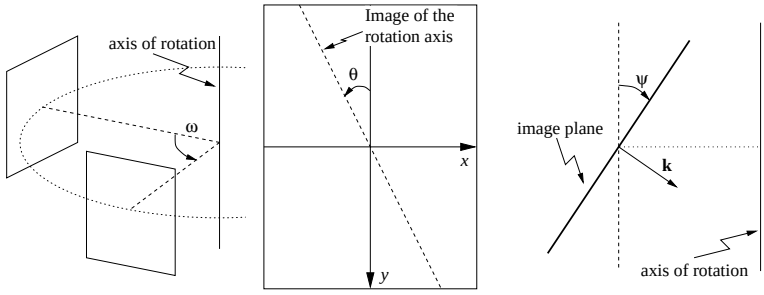

(a) (b) (c)

Figure 6: (a) The cameras are related by a rotation ω around a fixed axis. The angle θ shown in (b) corresponds to the angle between the vertical axis in image coordinates and the image of the axis of rotation. In (c) it can be seen that ψ is the angle between the axis of rotation and the image plane. Both ψ and θ do not change due to the rotation ω.

image, following the direction of $\mathbf{k}_1$ (see fig. 7(b)). Using elementary trigonometry, it is possible to show that the angle α will be given by

$$\alpha = -\arctan\left(\sin\psi \times \left(\frac{1-\cos\omega}{\sin\omega}\right)\right). \tag{8}$$

For non-zero cyclotorsion ($\theta \neq 0$), the angle $\gamma_{i,j}$ of epipolar lines at image i produced by

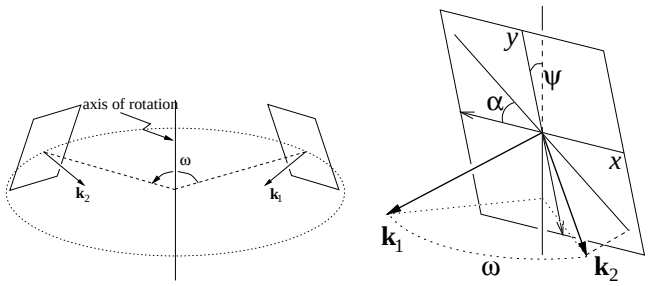

(a) (b)

Figure 7: The orientation α of the epipolar lines can be computed from the angles ψ and ω and the effect of θ can be considered separately. The vector $\mathbf{k}_2$ is projected in the image plane according the direction of $\mathbf{k}_1$.

image j will be given by $\gamma_{i,j} = -\theta + \alpha_{i,j}$, where $\alpha_{i,j}$ is the same as in (8) with $\omega = \omega_{i,j}$. If a sequence of n affine images of a surface rotating around a fixed axis is available, there will be $n+1$ parameters to be estimated: the 2 angles θ and ψ, and the $n-1$ angles $\omega_{i,i+1}$ between successive cameras. Obviously, the angle $\omega_{i,j}$ between the cameras i and j can be computed as $\sum_{k=0}^{j-i-1} \omega_{i+k,i+k+1}$, and it does not need to be represented using more parameters. It is worth emphasising the importance of (8). It allows for the representation of all the $n(n-1)$ orientations of the epipolar lines in a sequence of n affine cameras (all arrangements of pairs of images) with only $n+1$ parameters.

Further simplification can be achieved if the intrinsic parameters of the affine camera are assumed to be constant. In this case the image of the rotation axis, represented by

the line $\mathbf{l}$ in homogeneous coordinates, must be the same in all images. Every point $\mathbf{x}$ (also in homogeneous coordinates) in $\mathbf{l}$, taken at image i, must correspond to a point $\mathbf{x}$ with the same coordinates in image j. Let $\mathbf{F}_{i,j}$ be the fundamental matrix relating images i and j. Then, the equation $\mathbf{x}^{\mathrm{T}}\mathbf{F}_{i,j}\mathbf{x} = 0$ is satisfied *iff* the point $\mathbf{x}$ lies in the line $\mathbf{l}$. Assume now that two epipolar tangencies are available in each image i and j, which is equivalent to having at least one closed contour per image. The intersection of the pairs of correspondent epipolar lines (overlapping images i and j) provides two points $\mathbf{x}^1_{i,j}$ and $\mathbf{x}^2_{i,j}$ which satisfy $\mathbf{x}^{\mathrm{T}}\mathbf{F}_{i,j}\mathbf{x} = 0$, and thus must lie in $\mathbf{l}$. Thus, the sequence of images provides $n(n-1)$ points to determine the line $\mathbf{l}$. Since two points fix a line, $n(n-1)-2$ points remain, each one allowing one measurement for the estimation of the $(n+1)$-tuple of angles θ, ψ and $\{\omega_{i,i+1}\}_{i=1}^{n-1}$, henceforth denoted by $\mathbf{\Omega}$. Moreover, even if all the intersections of the epipolar lines are aligned, one further measurement is still possible, as the angle $\hat{\theta}$ between the line $\mathbf{l}$ and the vertical axis in image coordinates must be equal to θ. The result is that n images containing 2 epipolar tangencies each provide $n(n-1)-1$ measurements to estimate the $n+1$ parameters $\mathbf{\Omega}$, which can then be computed if $n \geq 3$. This is a great advantage over the results presented in [14, 6], where even for circular motion with *fixed rotation angle*, 4 images with 2 epipolar tangencies were still needed. The overall cost function for the estimation of $\mathbf{\Omega}$ is given by

$$C(\mathbf{\Omega}) = \sum_{i,j} (d^2(\mathbf{x}^{(1)}_{i,j}, \mathbf{l}) + d^2(\mathbf{x}^{(2)}_{i,j}, \mathbf{l})) + (\tan\hat{\theta} - \tan\theta)^2, \tag{9}$$

where $d(\mathbf{x}, \mathbf{l})$ is the orthogonal distance between the point $\mathbf{x}$ and the line $\mathbf{l}$. The technique to estimate the parameters of the circular motion of affine cameras is summarised in algorithm 1.

Algorithm 1 Estimation of the motion parameters from apparent contours.

track the contours using B-Splines;
initialise the angles $\mathbf{\Omega}$;
while not converge **do**
  compute the intersections $\mathbf{x}^{(1)}_{i,j}$ and $\mathbf{x}^{(2)}_{i,j}$ of epipolar tangents
  fit a line $\mathbf{l}(\mathbf{\Omega})$ to the points of intersection;
  compute the angle $\hat{\theta}$ between $\mathbf{l}$ and the vertical axis in image coordinates;
  compute the cost function $C(\mathbf{\Omega})$, as shown in (9);
  update $\mathbf{\Omega}$ to minimise $C(\mathbf{\Omega})$;
end while

3.2 Experimental Results

A preliminary experiment with synthetic data was carried out. Five images of an ellipsoid were generated [7] by successive rotations of a camera by $20°$. The optimisation method used to implement the algorithm described in algorithm 1 was the Broyden-Fletcher-Goldfarb-Shanno [12]. The computation of the derivatives of the cost function was done by finite differences, and each angle of $\mathbf{\Omega}$ was initialized within $7°$ of the ground truth. The epipolar lines and their intersections after convergence can be seen in fig 8.

To evaluate the effect of noise in the algorithm, each ellipse correspondent to the 5 images of the ellipsoid was sampled in 50 points. Uniform noise was added to each

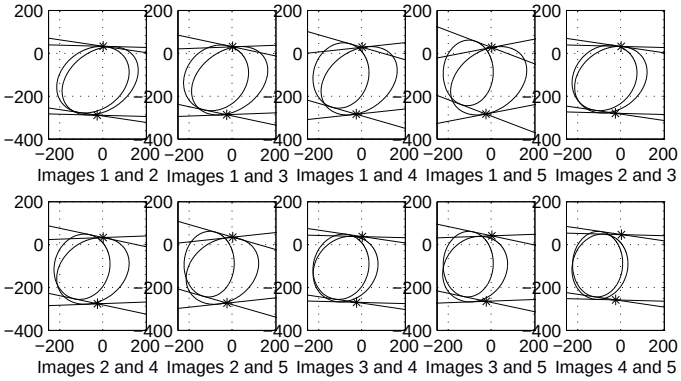

Figure 8: Images of the ellipses and epipolar lines after convergence. Each figure shows the overlapping of images i and j, for $i = 1, ..., 4$ and $j = i + 1, ..., 5$. The stars indicate the intersection of correspondent epipolar lines.

angle		θ	ψ	$\omega_{1,2}$	$\omega_{2,3}$	$\omega_{3,4}$	$\omega_{4,5}$
ground truth		5°	20°	20°	20°	20°	20°
initial guess		0°	27°	13°	20°	34°	20°
noise	iterations	error in θ	error in ψ	error in $\omega_{1,2}$	error in $\omega_{2,3}$	error in $\omega_{3,4}$	error in $\omega_{4,5}$
0.0	39.0000	0.0097°	0.2297°	0.2205°	0.2206°	0.2244°	0.2252°
0.1	38.8571	0.2148°	0.5457°	0.4666°	0.4825°	0.4981°	0.5066°
0.5	29.8444	1.0025°	0.9287°	0.8373°	0.7111°	0.7819°	0.6150°
1.0	26.0167	1.9926°	1.2045°	1.0959°	1.0314°	1.0880°	1.0838°
1.5	23.4906	3.0633°	1.7428°	1.4864°	1.7090°	1.7275°	1.6781°
2.0	21.7660	3.4753°	2.0284°	1.8631°	2.0974°	1.8470°	1.9657°

Table 1: After reaching the global minima valley, the algorithm promptly converges to the correct solution, and generally the angles describing the motion are correctly estimated within 2° of accuracy. Nevertheless, the presence of local minima and the insensitivity of the cost function to variations in ω make the search very difficult.

point, and a new ellipse was fitted back to the disturbed points. This experiment was reproduced 100 times for each different noise level, and the results *of the experiments that converged* are presented in table 1. The iterations presented for each noise level is the average number of iterations before convergence, and all errors are root mean square errors in degrees. The noise level is in pixels. Several problems were already found at this stage of the implementation of the algorithm. The expression for α, given by (8), is very insensitive to changes in ω for any practical value, e.g., $0 \leq \omega \leq \pi/2$. The effect of noise produces more disturbance in α than small variations in ω. Furthermore, the cost function C shown in (9) has many local minima points, some of them in regions with a radius of 5° around the global minima, making the initialisation step of the algorithm very critical.

4 Conclusions and Future Work

The technique for reconstruction proposed here is indeed well-known in stereo-vision, in the context of point and line features. Nevertheless, its application for curved surface reconstruction is original, and the results obtained were convincing. Moreover, the method is more flexible than previous ones, as it can cope with affine cameras. This makes it suitable to be used in conjunction with the motion estimation technique presented in sec-

tion 3.

The novel algorithm for motion estimation here introduced has a main advantage over previously proposed methods, in that it can cope with circular motion at a variable rotation angle even when only two epipolar tangencies are available in each image. This is a situation of great practical interest, since it corresponds to the motion of an object placed on a turntable spinning at unknown angle. Although the preliminary results are satisfactory, the algorithm is very sensitive to noise, and the presence of several local minima points in the cost function (9) makes the convergence difficult. The investigation of solutions to these problems are to be addressed in a future work.

References

[1] P.A. Beardsley, A. Zisserman, and D.W. Murray. Sequential updating of projective and affine structure from motion. *Int. Journal of Computer Vision*, 23(3):235–259, 1997.

[2] E. Boyer and M. O. Berger. 3D surface reconstruction using occluding contours. *Int. Journal of Computer Vision*, 22(3):219–233, 1997.

[3] R. Cipolla. The visual motion of curves and surfaces. *Phil. Trans. Royal Soc. London A*, 356:1103–1121, 1998.

[4] R. Cipolla and A. Blake. The dynamic analysis of apparent contours. In *Proc. 3rd Int. Conf. on Computer Vision*, pages 616–623, Osaka, Japan, 1990.

[5] R. Cipolla and A. Blake. Surface shape from the deformation of apparent contours. *Int. Journal of Computer Vision*, 9(2):83–112, 1992.

[6] R. Cipolla and P. R. S. Mendonça. The structure and motion of surfaces. In G. Picci and D.S. Gilliam, editors, *Dynamical Systems, Control, Coding, Computer Vision*, volume 25 of *Progress in Systems and Control Theory*, pages 369–391. Birkhauser, 1999.

[7] G. Cross and A. Zisserman. Quadric reconstruction from dual-space geometry. In *Proc. 6th Int. Conf. on Computer Vision*, pages 25–31, 1998.

[8] O. Faugeras. *Three-Dimensional Computer Vision: a Geometric Viewpoint.* MIT Press, 1993.

[9] A. W. Fitzgibbon, G. Cross, and A. Zisserman. Automatic 3D model construction for turn-table sequences. In *3D Structure from Multiple Images of Large-Scale Environments, European Workshop SMILE'98*, Lecture Notes in Computer Science 1506, pages 155–170, 1998.

[10] P.J. Giblin, F.E. Pollick, and J.E. Rycroft. Recovery of an unknown axis or rotation from the profiles of a rotating surface. *J. Opt. Soc. America A*, 11:1976–1984, 1994.

[11] H.C. Longuet-Higgins. A computer algorithm for reconstructing a scene from two projections. *Nature*, 293:133–135, 1981.

[12] D. G. Luenberger. *Linear and Nonlinear Programming.* Addison-Wesley, USA, second edition, 1984.

[13] Q-T. Luong and O. Faugeras. The fundamental matrix: Theory, algorithm, and stability analysis. *Int. Journal of Computer Vision*, 17:43–75, 1996.

[14] P. R. S. Mendonça and R. Cipolla. Structure and motion of surfaces: Affine and circular motion cases. In *Proc. Conf. Computer Vision and Pattern Recognition*, volume I, pages 9–14, Fort Collins, Colorado, 1999.

[15] F. E. Pollick. Perceiving shape from profiles. *Perception and Psychophysics*, 55(2):152–161, 1994.

[16] J. Porrill and S.B. Pollard. Curve matching and stereo calibration. *Image and Vision Computing*, 9(1):45–50, 1991.

[17] J.H. Rieger. Three dimensional motion from fixed points of a deforming profile curve. *Optics Letters*, 11:123–125, 1986.

[18] R. Szeliski and R. Weiss. Robust shape recovery from occluding contours using a linear smoother. *Int. Journal of Computer Vision*, 28(1):27–44, June 1998.

[19] R. Vaillant and O.D. Faugeras. Using extremal boundaries for 3D object modelling. *IEEE Trans. Pattern Analysis and Machine Intell.*, 14(2):157–173, 1992.

[20] Z. Zhang. Determining the epipolar geometry and its uncertainty: A review. *Int. Journal of Computer Vision*, 27(2):161–195, 1998.